Post-compression of a Q-switched laser in a glass-rod multi-pass cell

Journal of Physics: Photonics

OPEN ACCESS

RECEIVED
22 September 2025

REVISED
6 November 2025

ACCEPTED FOR PUBLICATION
14 November 2025

PUBLISHED
25 November 2025

PAPER

Post-compression of a Q-switched laser in a glass-rod multi-pass cell

Peer Biesterfeld[1,9], Arthur Schönberg[2,9], Marc Seitz[3,9], Nayla Jimenez[2,4,5], Tino Lang[2], Marcus Seidel[2,4,5], Prannay Balla[2], Lutz Winkelmann[2], Jyothish K Sunny[1], Sven Fröhlich[1], Philip Mosel[1], Ingmar Hartl[2], Francesca Calegari[3,6,7], Uwe Morgner[1,8], Milutin Kovacev[1,8], Christoph M Heyl[2,4,5,9] and Andrea Trabattoni[1,3,8,9,*]

[1] Leibniz University Hannover, Institute of Quantum Optics, Welfengarten 1, 30167 Hannover, Germany
[2] Deutsches Elektronen-Synchrotron DESY, Notkestraße 85, 22607 Hamburg, Germany
[3] Center for Free-Electron Laser Science CFEL, Deutsches Elektronen-Synchrotron DESY, Notkestraße 85, 22607 Hamburg, Germany
[4] Helmholtz-Institute Jena, Fröbelstieg 3, 07743 Jena, Germany
[5] GSI Helmholtzzentrum für Schwerionenforschung GmbH, Planckstraße 1, 64291 Darmstadt, Germany
[6] Department of Physics, Universität Hamburg, 22761 Hamburg, Germany
[7] The Hamburg Centre for Ultrafast Imaging, Universität Hamburg, 22607 Hamburg, Germany
[8] Cluster of Excellence PhoenixD (Photonics, Optics, and Engineering-Innovation Across Disciplines), 30167 Hannover, Germany
[9] These authors contributed equally to this work
[*] Author to whom any correspondence should be addressed.

E-mail: andrea.trabattoni@desy.de

Keywords: post-compression, nonlinear optics, ultrafast lasers, ultrafast optics, multi-pass cells

Supplementary material for this article is available online

Abstract

Q-switched lasers are compact, cost-effective, and highly pulse energy-scalable sources for nanosecond-scale laser pulses. The technology has been developed for many decades and is widely used in scientific, industrial and medical applications. However, their inherently narrow bandwidth imposes a lower limit on pulse duration—typically in the few-hundred-picosecond range—limiting the applicability of Q-switched technology in fields that require ultrafast laser pulses in the few-picosecond or femtosecond regime. In contrast, mode-locked lasers can produce broadband, ultrafast (<1 ps) pulses, but are complex, expensive, and typically require a large footprint. To bridge the parameter gap between these two laser platforms—in terms of pulse duration and achievable peak power—we here propose a Herriott-type multi-pass cell (MPC) based post-compression scheme for shortening the pulse durations of Q-switched lasers down to the ultrafast, picosecond regime. We experimentally demonstrate post-compression of 0.5 ns, 1 mJ pulses from a Q-switched laser to 24 ps using a compact glass-rod MPC for spectral broadening. We verify this result numerically and show that compression down to a few picoseconds is possible using the nanosecond MPC (nMPC). Through spectral filtering approaches, the nMPC suppresses detrimental nonlinear processes such as stimulated Raman scattering, which have set severe limitations for fiber-based post-compression of Q-switched lasers until today. Our results pave the way to cost-efficient and compact ultrafast laser platforms based on Q-switched laser technology.

1. Introduction

The continuous development of lasers has had a profound impact on our society. In particular, laser pulses with durations in the nano- ($1\text{ns} = 10^{-9}\text{s}$) to femtosecond ($1\text{fs} = 10^{-15}\text{s}$) range are routinely employed for microsurgery [1, 2] optical gas sensing [3], high-precision surface and volume material processing [4], or imaging of biological samples [5, 6]. Moreover, short-pulsed lasers are playing an indispensable role in fundamental research with applications ranging from the ultrafast spectroscopy of photo-induced electron dynamics in matter [7] via the manipulation of transient states in materials [8]

to recent breakthroughs in nuclear spectroscopy [9, 10]. Depending on the laser parameters, in particular the required peak power and pulse duration, different pulsed laser technologies are used, employing predominantly Q-switching or mode-locking schemes.

On the one hand, nanosecond pulses are typically generated using Q-switching methods [11–15]. Q-switched lasers can support high pulse energy (millijoule to joule), they are cost-efficient and can be built as robust and compact modules. Their peak power, however, is limited, hindering their effectiveness, for example, in material machining, dermatological treatment, or as driving light sources for nonlinear optical processes. On the other hand, shorter durations (pico- to femtoseconds) are the realm of mode-locked lasers [14, 16–18]. Such light sources provide pulses that enable the analysis of ultrafast phenomena at femtosecond time scales and furthermore support ultrahigh peak powers, which make them ideal for machining applications, at the expense, however, of high complexity, large footprints and much higher costs. In this context, the idea of compressing the duration of nano- to picosecond or sub-picosecond laser pulses is particularly appealing, as it offers a route to bridge the gap—at least in terms of pulse duration and achievable peak power—between Q-switching and mode-locking laser technologies.

In the last four decades, post-compression methods, i.e. technologies employing nonlinear optical processes to spectrally broaden and temporally compress the laser pulse, have tackled this challenge. Self-phase modulation (SPM) in hollow-core capillaries/fibers [19–21], photonic crystal fibers [22–24], or multi-pass cells (MPCs) [25–28] is used to compress mode-locked lasers even down to the few-femtosecond range. However, the compression of Q-switched lasers has proven more challenging. Compression methods exploiting stimulated Brillouin scattering (SBS) in bulk or liquid media or by propagation in long (>100 m) optical fibers, enabled to compress nanosecond lasers into the picosecond regime [29–33]. However, these efforts were limited in performance by phonon lifetime constraints or competing nonlinear effects—for instance, stimulated Raman scattering (SRS) - as well as in energy scalability, especially for the fiber based approaches. As a result, post-compressing Q-switched lasers to the parameter space of mode-locked lasers at millijoule-class pulse energies has not been achieved until now. Figure 1(a) illustrates this discussion, showing a representative set of post-compressed Q-switched and mode-locked lasers. The figure visualizes the input laser parameters (larger shapes) and the post-compressed output (smaller shapes), connected with dashed lines. The distribution of the displayed data points underlines a major parameter gap between the two laser technologies.

Here, we introduce a novel technology based on a bulk-rod Herriot-type MPC, that opens a route to compress lasers with few MW or sub-MW peak power into the pico- to femtosecond regime, approaching GW power levels. We experimentally demonstrate the technique by compressing a 0.5 ns pulse to 24 ps using a 10 cm-long fused silica (FS) rod as MPC nonlinear medium. Our simulations demonstrate that the method can scale to compression factors exceeding 100. Spectral filtering thereby prevents the rise of detrimental nonlinear processes including SRS and quasi-phase-matched four-wave-mixing (QPM-FWM). Our approach opens a perspective towards low-cost, compact, high-peak-power laser systems for novel implementations in science and industry. This includes, for example, the generation of high-flux extreme-ultraviolet (EUV) light, high-precision laser-driven material machining, or damage-free tissue treatment in dermatology.

2. Concept

Compressing the temporal duration of laser pulses relies on the concept of spectral broadening. Nonlinear optical processes such as SPM are employed for this purpose, being implemented in a variety of post-compression schemes [27]. Typically, a suitable regime of SPM implies the propagation of laser pulses at high peak power (usually ranging from 10 s of MW to the GW level) in nonlinear media such as gases or thin solid-state plates. To the best of our knowledge, pulses with a peak power down to about 8.7 MW have been post-compressed through SPM with an MPC [27]. In this framework, the post-compression of Q-switched pulses with nanosecond duration presents a main challenge: a typical Q-switched laser with a pulse energy of 1 mJ and a duration of 1 ns provides a peak power of only 1 MW, which prevents the post compression in conventional gas-filled or solid-state MPC designs. Long propagation in solid-core fibers with high optical nonlinearity may appear as a good mitigation strategy and has been employed to successfully post-compress nanosecond pulses in the nanojoule-energy regime [32, 42]. A different method involves using compression along with amplification in a fiber-based system. In this approach the compression, of short Q-switched laser pulses (100 ps) with an amplified energy of 0.1 mJ, to 2.7 ps has been demonstrated in a two stage setup [43, 44]. However, Raman and/or Brillouin scattering typically deteriorate the spectral broadening process, limiting energy-scalability especially for nanosecond pulses.

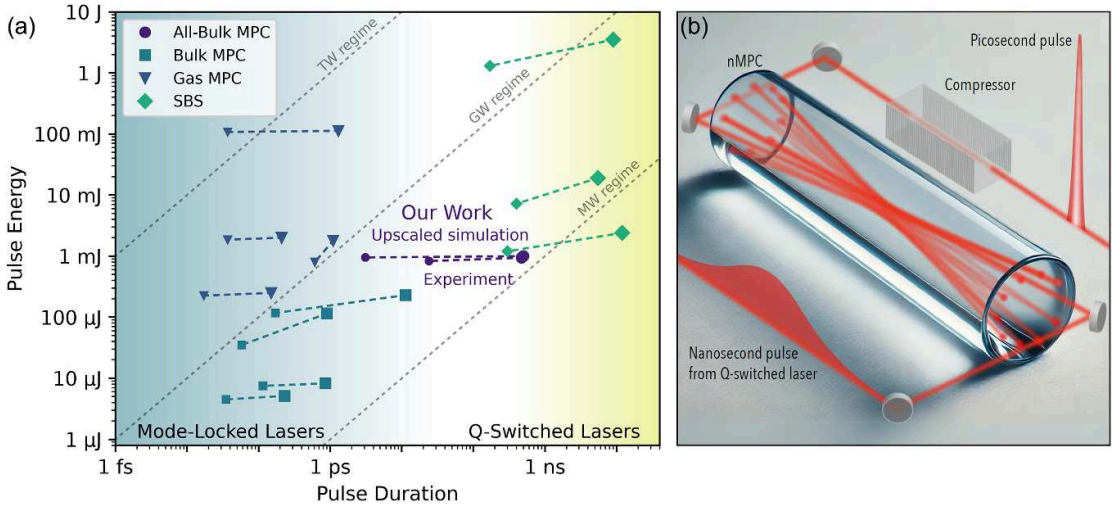

Figure 1. Post compression methods covering the parameter space from nanoseconds to femtoseconds. (a) Parameter overview of representative laser pulse post-compression works. Q-switched laser systems (green) have been post-compressed via SBS (diamonds), while gas-filled (triangles) or bulk (squares) MPCs are widely used for compressing mode-locked laser systems (blue) [26, 29, 30, 34–41]. Our work (purple) bridges the gap between these two laser regimes via post-compression of Q-switched lasers in a Herriott-type, bulk-rod MPC. The experimental output data point takes into account the output pulse duration measured at reduced energy, scaled to the full energy transmitted through the MPC. (b) Illustration of the proposed nanosecond MPC concept.

In order to overcome the above-mentioned limitations, we introduce a new type of MPC made completely out of glass such as FS. The monolithic MPC is equipped with high-reflectivity coated, curved surfaces acting as cavity mirrors (figure 1(b)). This type of MPC, dubbed nanosecond MPC (nMPC), presents unique advantages for long (nanosecond to hundreds of picoseconds) driving pulses. First, it provides both large nonlinear coefficients as well as long nonlinear interaction lengths while keeping the overall footprint of the setup compact. Second, while input pulses with pico- or femtosecond duration would suffer from the high dispersion in the bulk material, nanosecond pulses are insensitive to dispersion due to their narrow bandwidth. Third, the laser-induced damage threshold (LIDT) of the optical coating of the curved surfaces is much higher for nanosecond lasers than for shorter pulses, with values in the range of 10 s of J cm^{-2} [45, 46]. Consequently, MPC configurations with small beam sizes on the mirrors can be realized, thus allowing for many round trips and large spectral broadening factors. Fourth, the optical coatings can act as a spectral filter at each round trip, suppressing competing nonlinear optical processes such as Raman scattering and four-wave mixing that otherwise would strongly limit the pulse compressibility (further details in the discussion).

Based on this concept, simulations with an input pulse energy of 1 mJ, an input pulse duration of 0.5 ns of a Gaussian laser pulse and 150 round-trips ($N = 150, k = 91$), are carried out to demonstrate the potential of the nMPC. The simulation is performed using a symmetric split-step Fourier algorithm to solve the Unidirectional Pulse Propagation equation in (2+1) dimensions, assuming radial symmetry [47]. We consider a FS glass block with curved surfaces of $R = 10$ cm, length $L = 25.43$ cm and an MPC configuration parameter $k = 91$ [27]. The in/out coupling can be achieved through a small uncoated spot in one cell surface. By using a diameter of 3 inch (7.62 cm) for the curved surfaces, the necessary 150 reflections can be fit onto the curved surfaces. As an alternative route, a more dense round-trip pattern can be employed, overcoming geometric limitations of a simple circular pattern [48]. Figure 2 shows the results of the simulation. The spectral bandwidth of the input $\Delta\lambda_{10\mathrm{dB}} = 6$ pm increases by a factor of 220 to $\Delta\lambda_{10\mathrm{dB}} = 1.32$ nm, supporting a pulse duration of 2.2 ps (figure 2(a)). Following second-order phase compensation (103 ps^{-1}), a compressed pulse with a duration of 3.1 ps is obtained, showing very good compressibility. This results in a temporal compression by a factor of 161 and a final peak power of 82 MW (figure 2(b)). We note that large compression factors typically lead to the emergence of pedestals and limit the energy content in the main pulse, as shown in figure 2(b). However, strategies exist to mitigate this effect and optimize the pulse contrast, see the discussion section for more details.

Due to the inherent property of input-to-output beam imaging in MPCs [27], fluctuations in the input beam pointing are not amplified inside the nMPC, even for a large number of round trips (here $N = 150$) and the resulting long propagation distances. MPCs have been demonstrated to exhibit high stability even with a large number of reflections and long propagation distances [49]. Additionally, the

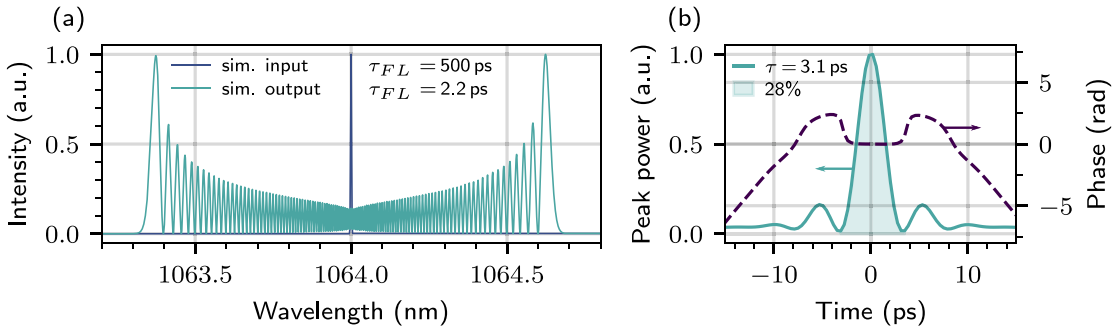

Figure 2. Simulated post-compression using the nMPC concept. (a) Input and output spectra demonstrating a high compression rate in the proposed full-bulk nMPC. (b) Corresponding compressed pulse, where the phase is compensated using GDD only.

all-bulk geometry mitigates the effects of ambient airflow as well as mechanical instability of the optical mounts, further increasing the stability of the system.

In the all-bulk scheme, the main sources of loss are the coated end facets of the bulk material and the absorption in the medium. With modern manufacturing methods, these losses can be kept very low, allowing the realization of such an MPC with an efficiency >90 %. Considering commercially available transmission gratings with efficiencies of >98% the total transmission of the setup can be in the order of 90 %. Alternatively, slightly less efficient but very compact compression can be achieved using a dispersive volume Bragg grating. The efficiency in the required parameter regime is >90% [50]. This allows for a total post-compression efficiency of >80% while maintaining a very small footprint.

The nMPC can potentially be further scaled to higher pulse energies and longer pulses, within limitations imposed mainly by SBS and the critical power of the material. While SBS imposes limits on the pulse duration and intensity, critical self-focusing can lead to beam collapse when the critical power of the material is exceeded. In the current nMPC configuration, the input pulse energy can be scaled up to 10 mJ when using a 4 ns long pulse, where the peak power is roughly half the critical power of FS ($P_{\mathrm{crit,FS}} \approx 5MW$) and the SBS limit is still not exceeded (see figure S4).

3. Experimental demonstration

We experimentally demonstrate the nMPC concept using a simplified setup which is schematically depicted in figure 3(a)). We employ a commercial Q-switched diode-pumped Nd:YAG laser (MPL2310, QS Lasers), emitting at 1064 nm. The passive Q-switching is achieved by a Cr:YAG crystal, resulting in the generation of pulses with a duration full-width at half maximum (FWHM) of 0.4 ns. With an ultracompact footprint (10 ×17 cm), the laser features a pulse energy of 2 mJ at a repetition rate of 100 Hz. The laser cavity is operated in single-mode emission upon thermal stabilization, yielding only (<0.1%) of energy in adjacent longitudinal modes. The single-mode contrast is further enhanced by using an Etalon filter with a free spectral range of 230 pm and a finesse of 41, resulting in an additional reduction of 24 dB for the adjacent modes, leading to a mode contrast of < 0.001%. The effect of multi-mode operation on the performance of the nMPC is discussed in detail in the supplemental (section S2).

For the sake of simplicity of this first test setup, we decomposed the monolithic bulk-rod nMPC into a set of two cavity mirrors, a large glass block, and an in-coupling scraper mirror. We use a 10 cm long block of anti-reflection coated, UV-FS as nonlinear medium, placed in the center between two concave mirrors with a radius of curvature of 0.1 m (figure 3(b)). The input beam is mode-matched to the MPC by a 3-lens telescope and is coupled into the cell by the scraper mirror with a width of 4 mm. The laser pulse undergoes 62 passes in the nMPC. Specifically, the MPC is configured with $N = 31$ and $k = 24$, where N defines the number of round trips and k specifies the chosen configuration which fulfills the re-entrance condition [27]. In this configuration, the linearly mode-matched MPC mode corresponds to a fluence of 0.3 J cm^{-2} on the cell mirrors and a peak intensity of $1{\cdot}10^{10}$W cm^{-2} at the focus. LIDT measurements have been conducted on the glass block, showing laser-induced damage inside the bulk for a driving peak intensity of $2{\cdot}10^{10}$W cm^{-2}. The in-coupled pulses have an energy of 0.94 mJ and a duration of 0.47 ns (FWHM), measured with an in-house developed second-order autocorrelator. The MPC transmission efficiency is measured to be 83%. This value is in good agreement with the calculated efficiency of 86%, considering the reflectivity of the cell mirrors and the FS bulk surfaces as specified by the manufacturer. The beam spatial quality is measured before and after the nMPC, showing a slight degradation of the mean M-square from 1.31 to 1.45 (see figure S1).

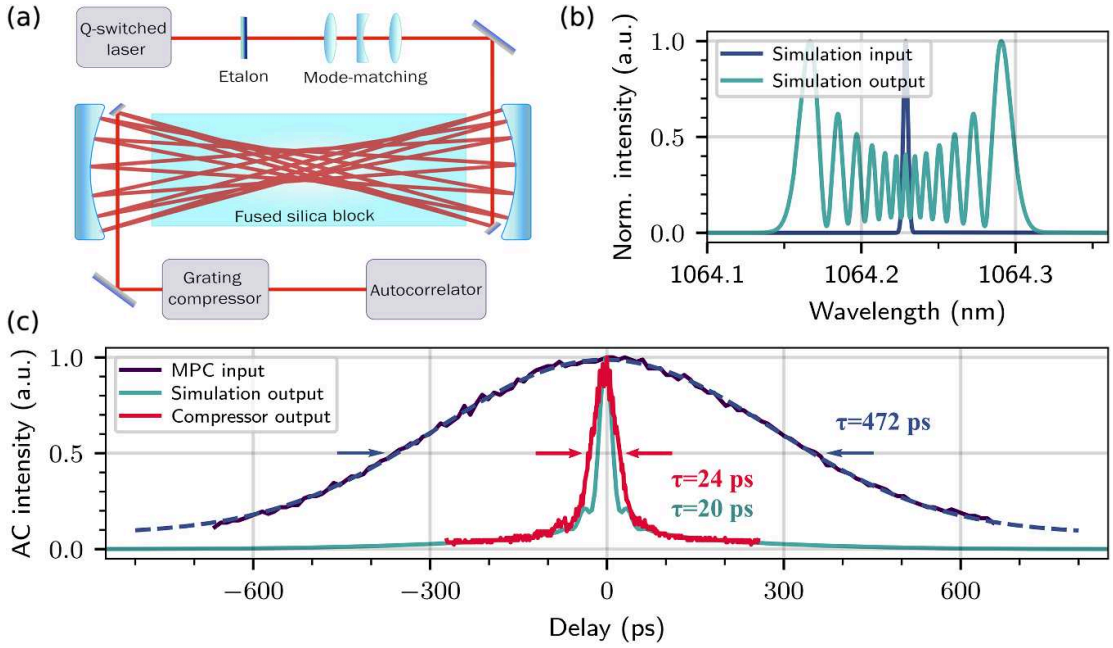

Figure 3. Experimental setup and results. (a) Schematic experimental setup including in particular an MPC using a 10 cm FS rod as a nonlinear medium. (b) Spectral broadening characteristics obtained via numerical (2+1)D simulation mimicking the experimental conditions. (c) Autocorrelation (AC) of the MPC input and compressor output pulse, along with the AC of the GDD-compensated simulated output. The pulse durations τ are obtained by fitting a Gaussian (input) and a Lorentzian (output) to the experimental data, taking the corresponding deconvolution factors into account.

Figure 3(b) shows the simulated SPM-driven spectral broadening occurring in the nMPC for the current experimental parameters. Starting from an input bandwidth of around 6 pm, an output bandwidth of 155 pm is obtained through SPM, corresponding to a transform-limited duration of 20 ps (FWHM). The spectral phase of the simulation output is compensated via GDD compensation ($-1370\,\mathrm{ps}^{-2}$), resulting in a pulse duration close to the Fourier-limited value and an energy content of 60% in the main pulse. Experimentally, spectral broadening is monitored using an Echelle spectrometer with a resolution of 35 pm at 1064 nm. Although this instrument is sufficient to show a signature of SPM, it is not able to resolve the broadened spectrum. For this reason, only the simulated spectra are reported in figure 3(b), while the experimental characterization of the input and output pulses was performed in the time domain. Following spectral broadening in the nMPC, the output beam is collimated and sent to a transmission-grating compressor, where the pulse is compressed in the time domain [27]. The compressor consists of two gratings with a line density of $1740\,\mathrm{l\,mm}^{-1}$, resulting in a total chirp of approx. $-1100\,\mathrm{ps}^{-2}$ and a limited efficiency of $\eta = 12\%$). We note that this compressor was used simply for availability reasons to demonstrate compressibility, disregarding efficiency. The used gratings can easily be replaced by tailored transmission gratings or by a chirped volume Bragg grating (CVBG). A CVBG can provide the required chirp while offering high efficiency ~90%, supporting high pulse energies and average powers exceeding 1 mJ and 250 W in a single compact optical element measuring a few centimeters in length [50].

The duration of the compressed pulses is measured to be 24 ps (FWHM), which is close to the simulated transform limit of 20 ps (figure 3(c)). The compression ratio, based on the measured input duration of 0.47 ns (FWHM), is approximately 20. This result demonstrates the effective compressibility of single-mode q-switched lasers in SPM-driven MPCs.

4. Discussion

Our proof-of-principle experiment demonstrates the nMPC concept and shows the first MPC-based compression of nanosecond-class laser pulses. The compressed pulses which can be obtained in our experiment using an improved compressor setup match the driving peak power range of post-compression setups already demonstrated in literature [26]. In addition, compression factor up-scaling to reach shorter output pulses in a single stage using our scheme appears feasible (see figure 2). Combining an nMPC with a conventional compression method thus holds promise to fully bridge the gap between nanosecond and femtosecond pulse durations, opening up a new class of femtosecond lasers.

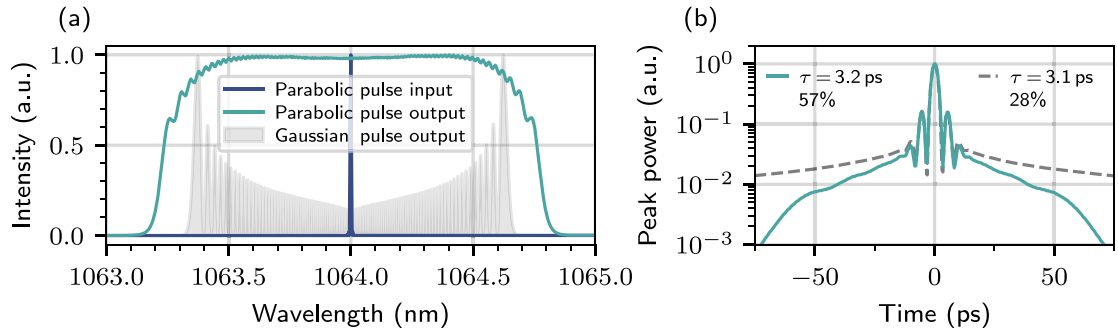

Figure 4. Simulated nMPC post-compression using a parabolic temporal pulse shape. (a) Spectral broadening of a temporally parabolic shaped pulse in comparison to a Gaussian pulse (identical to the data displayed in figure 2). (b) Corresponding GDD-compensated pulses, along with the energy fraction contained in the main pulse.

Taking into account future parameter scaling approaches, it is important to discuss the accessible parameter space supported by an nMPC. In this context, it is critical to consider that multiple detrimental processes can be triggered upon extreme spectral broadening in bulk media, and their contribution depends on the bandwidth of the input pulse. In this framework, we identify five major phenomena: temporal quality of post-compressed pulses, longitudinal mode beating of Q-switched lasers [51], SBS [52–54], SRS [54], and degenerate QPM-FWM [55]. We discuss the impact of these processes for post-compression in an nMPC along with suitable mitigation strategies.

The degradation of the temporal quality for high post compression factors in a single stage is a well-known challenge [56]. This effect is also seen in our simulations: it leads to a low energy content in the main pulse of only 28% for a compression factor of 161 by considering a Gaussian input pulse shape (figure 2). This effect results from the strongly modulated spectral shape and phase of an SPM broadened Gaussian pulse [57]. However, the temporal characteristics for large compression factors can be improved by separation into multiple stages, enhanced frequency chirping or nonlinear polarization ellipse rotation [57–59].

Another option is shaping the temporal intensity profile of the input pulse into a parabolic shape, which can lead to a high-contrast SPM-post-compressed pulse [60]. In the femtosecond regime, this is commonly realized by means of a spatial mask in the Fourier plane [61, 62]. In contrast, operating in the nanosecond regime makes it possible to employ direct temporal pulse-form shaping technology, which is readily available at sub-ns levels with ps resolution [63, 64].

Figure 4 shows this approach in a (2+1)D simulation with an input pulse energy of $E_\mathrm{p} = 0.5$ mJ, 225 round trips through the MPC and a B-integral per pass of $B_\mathrm{pass} = 0.2\pi$. The number of round trips N has been chosen to match the Fourier transform limit of the broadened spectrum displayed in figure 2 for direct comparison. All parameters not specified above are kept as in figure 2. The parabolic input pulse generates a much smoother output spectrum, increasing the energy content of the main pulse by a factor of 2. Our simulations indicate that a further improved energy content in the main pulse can be achieved for decreasing B_pass, compensated by an increased N.

The next challenge for Q-switched laser pulse compression is longitudinal mode beating, which can occur due to additional longitudinal modes emitted from the laser itself, a typical phenomenon for Q-switched lasers [65]. The resulting modulation of the temporal profile of the pulse occurring due to temporal mode interference can distort the phase of the SPM-broadened spectrum, degrading the compressibility of the pulse, as observed in our experiments (see section S2). Our numerical simulations reveal that an additional mode with an energy fraction of only 10^{-4} of the main pulse can already have severe effects on the output spectrum. Thus, mode cleaning before coupling into the nMPC becomes necessary.

Another challenge is SBS, which arises from the nonlinear interaction of an incoming light wave (pump) with the acoustic modes of the medium via electrostriction, generating a periodic modulation of the material density. For pulse energies exceeding a material-dependent threshold intensity, the laser pulse releases energy into a backward-propagating Stokes wave, which is frequency-shifted by a few GHz relative to the incoming wave [52–54]. SBS thus represents a potential loss channel for an nMPC. The SBS frequency shift is a material-dependent property. For FS this shift is equivalent to 16.3 GHz [66]. Following the formalism of transient Brillouin scattering ($\tau < 100$ ns) in fibers [67], it can be shown that the effective intensity for the nMPC example reported above is two orders of magnitude lower than the threshold intensity required for SBS, i,e. $I^\mathrm{eff}_\mathrm{nMPC}/I^\mathrm{th}_\mathrm{SBS} = 0.013$ (see figure S4). For the same intensity, the SBS threshold is instead surpassed when the input pulse duration is increased to $\tau \approx 5$ ns. In

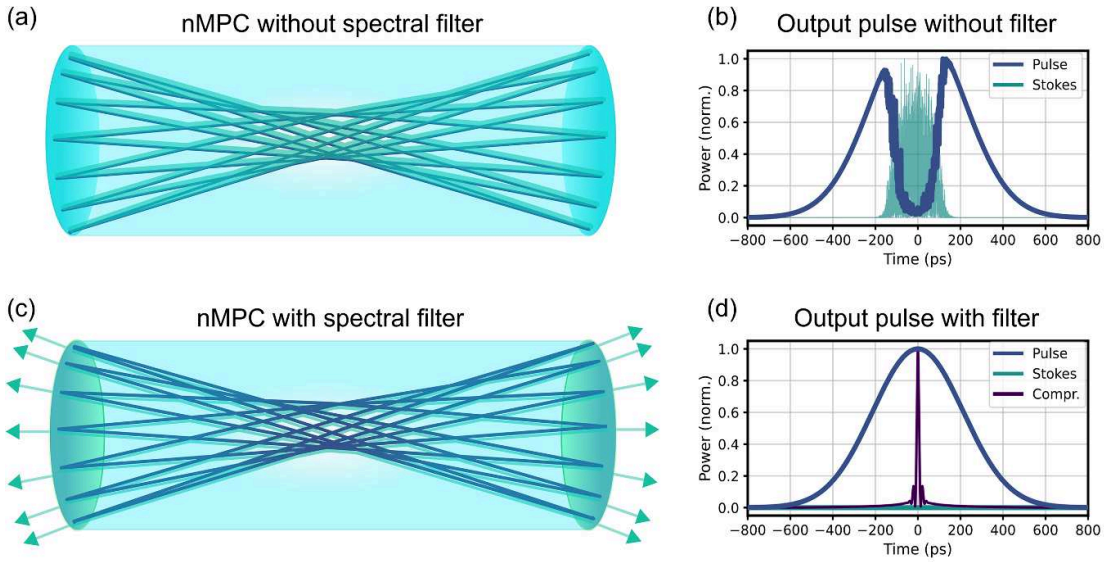

Figure 5. Impact and suppression of SRS in nMPC post-compression. (a) and (c) Illustration of the nMPC with (c) and without (a) spectral SRS filter. The transmitted Stokes components are pictorially indicated with arrows. (b) and (d) Corresponding simulated temporal pulse shapes following spectral broadening in the nMPC. Without filter, the pulse transfers energy to the Stokes field, leading to a distorted temporal pulse shape (b). This effect can be suppressed (d) using a suitable MPC mirror design, acting as spectral filter suppressing the Stokes pulse.

this case, SBS can be suppressed by reducing the peak power at the expense of the single-pass spectral broadening.

In addition to SBS, SRS can severely limit spectral broadening. SRS is an inelastic, stimulated scattering process in which photons are downshifted in energy by an amount determined by the vibrational modes of the medium [54]. In FS, the Stokes wave is frequency-down-shifted by about 13.6 THz [68]. Similar to SBS, the magnitude of SRS becomes important after exceeding a certain intensity threshold. Due to the large frequency shift, dispersion between the original pump pulse and the Stokes pulse can influence the dynamics of SRS [54]. SRS has been the major limiting factor of spectral broadening in fibers [69]. Although large broadening factors up to 80 have been demonstrated in fibers [32, 42], SRS limits the possible pulse energies to far below 1 μJ. While in our proof-of-principle experiment we did not observe any significant SRS onset, in the case of the upscaled simulation reported in figure 2, SRS becomes prominent (see equation (S6) in section S5). However, within the nMPC scheme the SRS contribution can be suppressed by using suitable MPC mirror coatings, acting as spectral filters for the Stokes pulse at each reflection.

Using FS as nonlinear material, the Stokes pulse of a laser pulse centered at 1064 nm appears at around 1112 nm and thus far outside the spectral range covered by the SPM-broadened spectrum, making spectral filtering possible. Figure 5 shows two simulated spectral broadening scenarios in an nMPC using 500 ps, 1 mJ pulses. Attenuating the Stokes field by only 30% per mirror reflection completely suppresses SRS and results in clean, compressible pulses (figures 5(c) and (d)).

Another limiting nonlinear effect is QPM-FWM, which can occur in MPCs with large broadening factors [55]. Similar to SRS, this effect can severely limit spectral broadening due to the generation of spectral side-bands, introducing strong modulations on the pulse in the temporal domain. We analyze this effect numerically and estimate its impact for nMPC post-compression (section S5), identifying a simple mitigation strategy. The location of the spectral side-bands depends on the dispersion properties of the nMPC, including the nonlinear medium and the mirrors, as well as on the MPC configuration. For the considered example case with the laser pulse centered at 1064 nm, the first QPM-FWM peaks appear at 1047 nm and 1082 nm. Similar to SRS, suitable optical coatings can be used to filter out both QPM-FWM induced spectral side-bands at each reflection and fully suppress their effect (see figure S7).

In the presented experiment, the moderate broadening factor of 20 resulted in the absence of the majority of the aforementioned detrimental effects, including SRS and QPM-FWM. However, our simulations reveal the importance of SRS and QPM-FWM suppression via spectral filtering for large spectral broadening factors (figures S5 and S7), indicating the importance of suitable mitigation strategies. We note that the (2+1)D simulation results presented in figures 2 and 4 do not include the effect of SRS and QFM-FWM for computational reasons. However, we also performed (1+1)D simulations with

the same parameters, while also considering SRS and QFM-FWM (see figure S7). In particular, we show that the use of suitable optical coatings effectively filters out and suppresses the contribution of SRS and QFM-FWM even for large compression factors, while maintaining a very high reflectivity (>99.98%) around the center wavelength of the laser.

5. Conclusion and outlook

We introduced a novel approach to compress Q-switched laser pulses using an nMPC, which uses a long glass rod as the nonlinear medium, as well as spectral filtering concepts to suppress detrimental nonlinear effects. Our approach enables efficient spectral broadening of low peak-power sources and extremely high compression factors, while also overcoming key limitations observed in fiber-based spectral broadening, such as SRS. Our proof-of-concept experiment demonstrates the compression of a 0.5 ns long pulse to a duration of 24 ps, with numerically validated scalability down to 3 ps. When combined with a second post-compression stage, the nMPC provides a bridge between nanosecond Q-switched lasers and femtosecond pulses. Our results open perspectives towards low-cost, high-peak-power ultrafast sources. Ultimately, the nMPC technology is promising to support a range of advanced applications, including the generation of high-flux EUV light for material characterization and ultrafast laser spectroscopy research, high-precision laser-driven material machining for industrial manufacturing, and damage-free tissue treatment in dermatology.

Data availability statement

All data that support the findings of this study are included within the article (and any supplementary files).

Supplementary data available at https://doi.org/10.1088/2515-7647/ae1fc4/data1.

Acknowledgments

Views and opinions expressed are however those of the author(s) only and do not necessarily reflect those of the European Union or the European Research Council Executive Agency. Neither the European Union nor the granting authority can be held responsible for them.

Funding

Cluster of Excellence PhoenixD (DFG EXC 2181); Cluster of Excellence 'CUI: Advanced Imaging of Matter' (EXC 2056, 390 715 994); European Innovation Council Pathfinder Project 'NanoXCAN' (101 047 223); Helmholtz Young Investigator Group (VH-NG-1603); Deutsche Forschungsgemeinschaft (545 612 524); Helmholtz-Lund International Graduate School (HELIOS) (HIRS-0018); European Research Council 'SoftMeter' (101 076 500); Bundesministerium für Forschung, Technologie und Raumfahrt (BMFTR) (13N16678); Gottfried Wilhelm Leibniz Universität Hannover; Deutsches Elektronen-Synchrotron DESY; Helmholtz-Institute Jena; Helmholtz Association.

Author contributors

CH and AT conceived the initial idea and supervised the project. PBi, AS, MS, NJ, TL, JKS, SF, PM performed the experiment. PBi and AS carried out the data analysis, as well as the (1+1)D and the (2+1)D simulations supporting the concept and the experiment. PBi, AS, MS, CH, and AT drafted to writing the manuscript. All authors discussed the results and contributed to the manuscript.

ORCID iDs

Peer Biesterfeld 0009-0003-3125-3051
Arthur Schönberg 0009-0001-4189-9978
Marc Seitz 0009-0004-2251-1298
Nayla Jimenez 0000-0002-8317-3585
Christoph M Heyl 0000-0003-2133-5224
Andrea Trabattoni 0000-0002-0187-9075

References

[1] Linz N, Freidank S, Liang X-X and Vogel A 2023 *Ultrafast Laser Nanostructuring: The Pursuit of Extreme Scales* (Springer) pp 1217–45
[2] Skorczakowski M *et al* 2010 Mid-infrared Q-switched Er:YAG laser for medical applications *Laser Phys. Lett.* **7** 498
[3] Hodgkinson J and Tatam R P 2012 Optical gas sensing: a review *Meas. Sci. Technol.* **24** 012004
[4] Sugioka K and Cheng Y 2014 Ultrafast lasers - reliable tool for advanced material processing *Light Sci. Appl.* **3** e149–149
[5] Fan S, Wang S, Yang C, Wise F and Kong L 2023 Advances of mode-locking fiber lasers in neural imaging *Adv. Opt. Mater.* **11** 2202945
[6] Lefort C 2017 A review of biomedical multiphoton microscopy and its laser sources *J. Phys. D: Appl. Phys.* **50** 423001
[7] Cederbaum L and Zobeley J 1999 Ultrafast charge migration by electron correlation *Chem. Phys. Lett.* **307** 205–10
[8] Nicoletti D, Casandruc E, Laplace Y, Khanna V, Hunt C R, Kaiser S, Dhesi S S, Gu G D, Hill J P and Cavalleri A 2014 Optically induced superconductivity in striped $La_{2-x}Ba_xCuO_4$ by polarization-selective excitation in the near infrared *Phys. Rev. B* **90** 100503
[9] Tiedau J *et al* 2024 Laser excitation of the Th-229 nucleus *Phys. Rev. Lett.* **132** 182501
[10] Elwell R, Schneider C, Jeet J, Terhune J E S, Morgan H W T, Alexandrova A N, Tan H B T, Derevianko A and Hudson E R 2024 Laser excitation of the ^{229}Th nuclear isomeric transition in a solid-state host *Phys. Rev. Lett.* **133** 013201
[11] Wang Y and Xu C-Q 2007 Actively Q-switched fiber lasers: switching dynamics and nonlinear processes *Prog. Quantum Electron.* **31** 131–216
[12] Chen X, Wang N, He C and Lin X 2023 Development of all-fiber nanosecond oscillator using actively Q-switched technologies and modulators *Opt. Laser Technol.* **157** 108709
[13] Al-Hiti A S, Yasin M and Harun S W 2022 Nanosecond Q-switched laser with PEDOT: PSS saturable absorber *Appl. Opt.* **61** 1292–9
[14] Paschotta R 2008 *Field Guide to Laser Pulse Generation* (SPIE Press)
[15] Zhou Y, Li X, Xu H, Yan R, Jiang Y, Fan R and Chen D 2021 High-pulse-energy passively Q-switched sub-nanosecond MOPA laser system operating at kHz level *Opt. Express* **29** 17201–14
[16] Kues M, Reimer C, Wetzel B, Roztocki P, Little B E, Chu S T, Hansson T, Viktorov E A, Moss D J and Morandotti R 2017 Passively mode-locked laser with an ultra-narrow spectral width *Nat. Photon.* **11** 159–62
[17] Kim J and Song Y 2016 Ultralow-noise mode-locked fiber lasers and frequency combs: principles, status and applications *Adv. Opt. Photon.* **8** 465
[18] Han Y, Guo Y, Gao B, Ma C, Zhang R and Zhang H 2020 Generation, optimization and application of ultrashort femtosecond pulse in mode-locked fiber lasers *Prog. Quantum Electron.* **71** 100264
[19] Nagy T, Simon P and Veisz L 2020 High-energy few-cycle pulses: post-compression techniques *Adv. Phys. X* **6** 1845795
[20] Frosz M H, Bradley T D, Habib M S, Markos C, Travers J and Wang Y 2024 Editorial: advances and applications of hollow-core fibers *IEEE J. Sel. Top. Quantum Electron.* **30** 1001003
[21] Nisoli M, De Silvestri S and Svelto O 1996 Generation of high energy 10 fs pulses by a new pulse compression technique *Appl. Phys. Lett.* **68** 2793–5
[22] Gebhardt M, Gaida C, Hädrich S, Stutzki F, Jauregui C, Limpert J and Tünnermann A 2015 Nonlinear compression of an ultrashort-pulse thulium-based fiber laser to sub-70 fs in Kagome photonic crystal fiber *Opt. Lett.* **40** 2770–3
[23] Heidt A M, Rothhardt J, Hartung A, Bartelt H, Rohwer E G, Limpert J and Tünnermann A 2011 High quality sub-two cycle pulses from compression of supercontinuum generated in all-normal dispersion photonic crystal fiber *Opt. Express* **19** 13873–9
[24] Mak K F, Travers J C, Joly N Y, Abdolvand A and Russell P S J 2013 Two techniques for temporal pulse compression in gas-filled hollow-core kagomé photonic crystal fiber *Opt. Lett.* **38** 3592–5
[25] Schulte J, Sartorius T, Weitenberg J, Vernaleken A and Russbueldt P 2016 Nonlinear pulse compression in a multi-pass cell *Opt. Lett.* **41** 4511–4
[26] Weitenberg J, Vernaleken A, Schulte J, Ozawa A, Sartorius T, Pervak V, Hoffmann H-D, Udem T, Russbüldt P and Hänsch T W 2017 Multi-pass-cell-based nonlinear pulse compression to 115 fs at 7.5 μJ pulse energy and 300 W average power *Opt. Express* **25** 20502–10
[27] Viotti A-L, Seidel M, Escoto E, Rajhans S, Leemans W P, Hartl I and Heyl C M 2022 Multi-pass cells for post-compression of ultrashort laser pulses *Optica* **9** 197–216
[28] Hanna M, Délen X, Lavenu L, Guichard F, Zaouter Y, Druon F and Georges P 2017 Nonlinear temporal compression in multipass cells: theory *J. Opt. Soc. Am. B* **34** 1340–7
[29] Tarasov A A and Chu H 2017 Subnanosecond Nd:YAG laser with multipass cell for SBS pulse compression *Solid State Lasers Xxvi: Technology and Devices* Ed W A Clarkson and R K Shori (*Proc. SPIE*) **10082** 100820Q
[30] Feng C, Xu X and Diels J-C 2017 High-energy sub-phonon lifetime pulse compression by stimulated Brillouin scattering in liquids *Opt. Express* **25** 12421–34
[31] Maier M, Kaiser W and Giordmaine J A 1966 Intense Light Bursts in the Stimulated Raman Effect *Phys. Rev. Lett.* **17** 26
[32] Johnson A M, Stolen R H and Simpson W M 1984 80× single-stage compression of frequency doubled Nd:yttrium aluminum garnet laser pulses *Appl. Phys. Lett.* **44** 729–31
[33] Mollenauer L F, Stolen R H, Gordon J P and Tomlinson W J 1983 Extreme picosecond pulse narrowing by means of soliton effect in single-mode optical fibers *Opt. Lett.* **8** 289–91
[34] Weitenberg J, Saule T, Schulte J and Rubbuldt P 2017 Nonlinear pulse compression to sub-40 fs at 4.5 μJ pulse energy by multi-pass-cell spectral broadening *IEEE J. Quantum Electron.* **53** 8600204
[35] Song J, Wang Z, Renchong L, Xianzhi W, Teng H, Zhu J and Wei Z 2021 Generation of 172 fs pulse from a Nd:YVO4 picosecond laser by using multi-pass-cell technique *Appl. Phys. B* **127** 50
[36] Seidel M *et al* 2022 Ultrafast MHz-rate burst-mode pump-probe laser for the FLASH FEL facility based on nonlinear compression of ps-level pulses from an yb-amplifier chain *Laser Photon. Rev.* **16** 2100268
[37] Silletti L *et al* 2023 Dispersion-engineered multi-pass cell for single-stage post-compression of an ytterbium laser *Opt. Lett.* **48** 1842–5
[38] Ueffing M, Reiger S, Kaumanns M, Pervak V, Trubetskov M, Nubbemeyer T and Krausz F 2018 Nonlinear pulse compression in a gas-filled multipass cell *Opt. Lett.* **43** 2070–3
[39] Viotti A L, Alisauskas S, Wahid A B, Balla P, Schirmel N, Manschwetus B, Hartl I and Heyl C M 2021 60 fs, 1030 nm FEL pump-probe laser based on a multi-pass post-compressed Yb:YAG source *J. Synchrotron Radiat.* **28** 36–43

[40] Kaumanns M, Kormin D, Nubbemeyer T, Pervak V and Karsch S 2021 Spectral broadening of 112 mJ, 1.3 ps pulses at 5 kHz in a LG10 multipass cell with compressibility to 37 fs *Opt. Lett.* **46** 929–32
[41] Feng C, Xu X and Diels J-C 2014 Generation of 300 ps laser pulse with 1.2 J energy by stimulated Brillouin scattering in water at 532 nm *CLEO: 2014* SM2F.7 (https://doi.org/10.1364/CLEO_SI.2014.SM2F.7)
[42] Kafka J D, Kolner B H, Baer T and Bloom D M 1984 Compression of pulses from a continuous-wave mode-locked Nd:YAG laser *Opt. Lett.* **9** 505
[43] Steinmetz A, Eidam T, Nodop D, Limpert J and Tünnermann A 2011 Nonlinear compression of Q-Switched laser pulses to the realm of ultrashort durations *Opt. Express* **19** 3758–64
[44] Steinmetz A, Jansen F, Stutzki F, Lehneis R, Limpert J and Tünnermann A 2012 Sub-5-ps, multimegawatt peak-power pulses from a fiber-amplified and optically compressed passively Q-switched microchip laser *Opt. Lett.* **37** 2550–2
[45] Niemz M H 1995 Threshold dependence of laser-induced optical breakdown on pulse duration *Appl. Phys. Lett.* **66** 1181–3
[46] Atkočaitis E, Smalakys L and Melninkaitis A 2022 Pulse temporal scaling of lidt for anti-reflective coatings deposited on lithium triborate crystals *Opt. Express* **30** 28401
[47] Couairon A, Brambilla E, Corti T, Majus D, Ramirez-Gongora O and Kolesik M 2011 Practitioner's guide to laser pulse propagation models and simulation *Eur. Phys. J. Spec. Top.* **199** 5–76
[48] Robert C 2007 Simple, stable and compact multiple-reflection optical cell for very long optical paths *Appl. Opt.* **46** 5408–18
[49] Schönberg A *et al* 2025 Compact, folded multi-pass cells for energy scaling of post-compression *Photon. Res.* **13** 761
[50] Glebov L, Smirnov V, Rotari E, Cohanoschi I, Glebova L, Smolski O, Lumeau J, Lantigua C and Glebov A 2014 Volume-chirped bragg gratings: monolithic components for stretching and compression of ultrashort laser pulses *Opt. Eng., Bellingham* **53** 051514
[51] Corless J D, West J A, Bromage J and Stroud C R 1997 Pulsed single-mode dye laser for coherent control experiments *Rev. Sci. Instrum.* **68** 2259–64
[52] Chiao R Y, Townes C H and Stoicheff B P 1964 Stimulated Brillouin Scattering and Coherent Generation of Intense Hypersonic Waves *Phys. Rev. Lett.* **12** 592–5
[53] Armandillo E and Proch D 1983 Highly efficient, high-quality phase-conjugate reflection at 308 nm using stimulated Brillouin scattering *Opt. Lett.* **8** 523–5
[54] Agrawal G P 2013 *Nonlinear fiber optics Engineering Professional Collection* 5th edn (Academic)
[55] Hanna M, Daher N, Guichard F, Délen X and Georges P 2020 Hybrid pulse propagation model and quasi-phase-matched four-wave mixing in multipass cells *J. Opt. Soc. Am. B* **37** 2982–8
[56] Escoto E, Viotti A-L, Alisauskas S, Tünnermann H, Hartl I and Heyl C M 2022 Temporal quality of post-compressed pulses at large compression factors *J. Opt. Soc. Am. B* **39** 1694–702
[57] Escoto E, Pressacco F, Jiang Y, Rajhans S, Khodakovskiy N, Hartl I, Seidel M, Heyl C M and Tünnermann H 2024 Improved temporal characteristics for post-compressed pulses via application-tailored nonlinear polarization ellipse rotation *Opt. Lett.* **49** 6841–4
[58] Pfaff Y. et al 2022 Nonlinear pulse compression of a thin-disk amplifier and contrast enhancement via nonlinear ellipse rotation *Opt. Express* **30** 10981–90
[59] Benner M, Karst M, Mendez C A, Stark H and Limpert J 2023 Concept of enhanced frequency chirping for multi-pass cells to improve the pulse contrast *J. Opt. Soc. Am. B* **40** 301–5
[60] Nguyen D, Piracha M U, Mandridis D and Delfyett P J 2011 Dynamic parabolic pulse generation using temporal shaping of wavelength to time mapped pulses *Opt. Express* **19** 12305–11
[61] Monmayrant A, Weber S and Chatel B 2010 A newcomer's guide to ultrashort pulse shaping and characterization *J. Phys. B: At. Mol. Opt. Phys.* **43** 103001
[62] Lefort C, Kalashyan M, Ducourthial G, Mansuryan T, O'Connor R P and Louradour F 2014 Sub-30-fs pulse compression and pulse shaping at the output of a 2-m-long optical fiber in the near-infrared range *J. Opt. Soc. Am. B* **31** 2317–24
[63] Rogers C E and Gould P L 2016 Nanosecond pulse shaping at 780 nm with fiber-based electro-optical modulators and a double-pass tapered amplifier *Opt. Express* **24** 2596–606
[64] Meijer R A, Stodolna A S, Eikema K S E and Witte S 2017 High-energy Nd:YAG laser system with arbitrary sub-nanosecond pulse shaping capability *Opt. Lett.* **42** 2758–61
[65] Sooy W R 1965 The natural selection of modes in a passive Q-switched laser *Appl. Phys. Lett.* **7** 36–37
[66] Bai Z, Yuan H, Liu Z, Xu P, Gao Q, Williams R J, Kitzler O, Mildren R P, Wang Y and Lu Z 2018 Stimulated Brillouin scattering materials, experimental design and applications: A review *Opt. Mater.* **75** 626–45
[67] Keaton G L, Leonardo M J, Byer M W and Richard D J 2014 Stimulated Brillouin scattering of pulses in optical fibers *Opt. Express* **22** 13351–65
[68] Stolen R H, Tomlinson W J, Haus H A and Gordon J P 1989 Raman response function of silica-core fibers *J. Opt. Soc. Am. B* **6** 1159
[69] Nakashima T, Nakazawa M, Nishi K and Kubota H 1987 Effect of stimulated Raman scattering on pulse-compression characteristics *Opt. Lett.* **12** 404–6